Supporting Information

Sherman et al. 10.1073/pnas.1323516111

SI Materials and Methods

Strains and Growth Conditions for Genetics Experiments. Strains are listed in Table S1. Unless indicated, cells were grown in LB at 37 °C (1). For plates and top agar, LB was supplemented with 1.5% and 0.75% (wt/vol) agar, respectively. When necessary, ampicillin (150 μg/mL), kanamycin (30 μg/mL), carbenicillin (50 μg/mL), X-Gal (33 μg/mL), and isopropyl-β-D-1-thiogalactopyranoside (IPTG; 0.16 mM) were added to growth media.

Construction of Chromosomal *lptB* Deletions. Primers used for this study are listed in Tables S2 and S3. A chromosomal deletion of *lptB* and replacement with a kanamycin-resistance cassette (Δ*lptB*::*kan* allele), where the region from the second codon to the stop codon of *lptB* is deleted, was constructed using recombineering in DY378 (2) carrying pWSK29LptCAB (3). For recombineering, a PCR product obtained using primers 5LptBP1 and 3LptBP2, and pKD4 as a template (4), was introduced into NR1818 by electroporation. Kanamycin-resistant recombinants (NR1846) were obtained, and the presence of the Δ*lptB*::*kan* allele was confirmed by PCR. The Δ*lptB* allele was obtained by excising the kanamycin resistance cassette from Δ*lptB*::*kan* using pCP20 as previously described (5). When necessary, the Δ*lptB* allele was cotransduced with *tet2*, a mini-Tn*tet* transposon chromosomal insertion located 68 bp upstream of *yhcG* in the *yhcF–G* intergenic region.

Plasmid Construction. Plasmid pET23/42LptB was constructed by mutagenizing pET23/42LptB-His_8 (6) to insert a stop codon before the region encoding the His_8 tag using primers LptB-MinusCHis-f and LptB-MinusCHis-r. Site-directed mutagenesis (SDM) was performed using KOD Hot Start DNA Polymerase (Novagen). The PCR product of the SDM reaction was digested with DpnI (New England Biolabs) and introduced into NovaBlue competent cells by heat shock. Transformants were selected in media containing carbenicillin. After confirming plasmid DNA sequence, mutagenized plasmids were introduced into NR2050 and NR754 using chemical transformation (7).

Plasmid pRC7KanLptB, a kanamycin-resistant derivative of pRC7 (8) carrying a wild-type *lptB* allele, was constructed in two steps. First, the ampicillin-resistant parent plasmid pRC7LptB was constructed by introducing the *lptB* allele into pRC7. To do this step, a PCR product generated using primers 5LptBEcoRI and 3LptBHindIII, and NR754 chromosomal DNA as a template, was introduced into pRC7 digested by EcoRI and HindIII enzymes (New England Biolabs). DH5α transformants were selected in growth medium containing 25 μg/mL ampicillin. The resulting plasmid, pRC7LptB, was introduced into DY378 (2) for recombineering to replace the ampicillin-resistant marker with one conferring resistance to kanamycin. In order to do this step, the kanamycin resistance cassette of pKD4 (4) was amplified by PCR using primers blaP1 and blaP2, and was introduced into NR1926. The resulting kanamycin-resistant strain, NR1931, harbors the recombinant plasmid pRC7KanLptB.

All *lptB* and *lptB-his* mutant alleles were constructed by mutagenizing either pET23/42LptB or pET23/42LptB-His_8 using SDM with PfuTurbo (Agilent Technologies, Inc.) or KOD Hot Start DNA Polymerase. PCR products of SDM reactions were digested with DpnI and introduced into NovaBlue or DH5α cells via electroporation. Transformants were selected in media containing ampicillin. After confirming plasmid DNA sequence, mutagenized plasmids were introduced into NR2050 and NR754 using chemical transformation, as described above.

Plasmid pCDFDuet-His_6LptB-LptFG was constructed in three steps. First, the parent plasmid pCDFDuet-LptFG was prepared by digesting pCDFDuet-LptCABHis_6-LptFG (9) with NcoI (New England Biolabs) and EcoRI enzymes to remove the DNA segment encoding *lptCAB-his* from the first multiple cloning site. The parent plasmid, pCDFDuet-LptFG, was gel-purified and used for subsequent steps. A digested PCR product generated using primers N-NcoI-His_6LptB and C-LptB-EcoRI, and pET23/42LptB as a template, was used to ligate a *his-lptB* allele into the first multiple cloning site of the parent plasmid. The ligation product was transformed into NovaBlue competent cells by heat shock, and transformants were selected in media containing spectinomycin (50 μg/mL). Plasmids were purified from individual colonies and sequenced.

pET22/42LptC was constructed by amplifying the *lptC* allele using primers N-NdeI-LptC and C-LptC-HindIII, and pCDFDuet-LptCABHis_6-LptFG as a template. The amplified fragment was digested with NdeI (New England Biolabs) and HindIII enzymes and inserted into a digested pET22/42 expression vector (10).

Functionality Tests of Mutant *lptB* Alleles. To assess the functionality of mutant *lptB* alleles, we developed a system to determine whether LptB variants complement the loss of a wild-type *lptB* allele. The system uses two types of compatible plasmids. One plasmid carries the mutant *lptB* allele to be tested. Specifically, we used a set of pET23/42LptB and pET23/42LptB-His_8 derivatives. The second plasmid, pRC7KanLptB, carries a wild-type allele of *lptB* and *lacZ*. Because pRC7KanLptB is defective in plasmid-partitioning functions, it is easily lost in a population of cells in the absence of selection (8). Therefore, when pRC7KanLptB is introduced into a wild-type strain, it is lost from the population unless kanamycin is present. However, pRC7KanLptB is stably maintained even in the absence of kanamycin in cells where the chromosomal *lptB* allele has been deleted because, in these *lptB* mutant cells, LptB itself is a selectable trait for plasmid maintenance. Maintenance of pRC7KanLptB can be easily determined by monitoring the LacZ activity derived from pRC7KanLptB on solid medium containing X-Gal. Cells that are viable in the absence of pRC7KanLptB form white or sectored white/blue colonies, whereas those that can only survive if they contain pRC7KanLptB form blue colonies. In our system, we therefore used a Δ*lptB* strain carrying pRC7KanLptB (NR2050) as a reporter strain for the functionality of *lptB* alleles carried by pET23/42LptB and pET23/42LptB-His_8 derivatives. If pET23/42LptB and pET23/42LptB-His_8 derivatives encode a functional *lptB* allele, colonies appear white or sectored in the presence of X-Gal; however, if they encode a nonfunctional *lptB* allele, colonies appear blue. We also confirmed functionality data obtained using this system by testing whether we could delete the chromosomal wild-type *lptB* allele from strains carrying pET23/42LptB and pET23/42LptB-His_8 derivatives by P1 transduction using a Δ*lptB*::*kan* strain as donor (strain NR1890) and selecting for kanamycin resistance.

Outer Membrane Permeability Tests. To determine whether functional alleles are wild-type or partial loss-of-function alleles, we assessed the outer membrane (OM) permeability of haploid strains carrying a Δ*lptB* chromosomal allele and a functional allele encoded by either a pET23/42LptB or pET23/42LptB-His_8 derivative. To identify alleles that confer dominant-negative phenotypes, we assessed the OM permeability of NR754-derived, merodiploid strains carrying the wild-type *lptB* allele at the native

chromosomal locus and a mutant *lptB* allele encoded by either a pET23/42LptB or pET23/42LptB-His_8 derivative. OM permeability was probed by determining the sensitivity to hydrophobic antibiotics using disk diffusion assays (11). Disk diffusion assays were performed by pouring a mixture of 50 μL of an overnight culture and 4 mL of LB top agar over LB agar plates. After top agar solidified, 6-mm antibiotic disks (BD BBL Sensi-Disk Susceptibility Test Disks) containing bacitracin (10 international units), novobiocin (30 μg), erythromycin (15 μg), and rifampicin (5 μg) were placed on top. After overnight incubation at 37 °C, zones of clearance around disks were measured.

LptB Levels Analysis. LptB protein levels were monitored by immunoblotting using anti-LptB antisera. This LptB polyclonal antiserum also contains antibodies that recognize the OM protein OmpA, which was used as a control for sample preparation and loading onto gels. Cultures were grown overnight, and their OD_{600} was measured. A 100-μL sample from overnight cultures was pelleted, and cells were resuspended in a volume (in mL) of Laemmli sample buffer equivalent to the value of $OD_{600}/100$. Samples were boiled for 10 min, and 10 μL was loaded onto 12% or 15% (for samples from merodiploid strains carrying pET23/42LptB-His_8 derivatives) SDS polyacrylamide gels. Proteins were transferred onto Potran nitrocellulose membranes (Whatman) that were probed with LptB antiserum (1:20,000 dilution) and anti–rabbit-HRP antibodies (1:10,000 dilution; GE Amersham). Signal was developed with Clarity Western ECL Substrate (Bio-Rad) using a ChemiDoc XRS+ system and ImageLab 3.0 software (BioRad).

Affinity Purification. To perform affinity purifications of LptB variants, the reported method was slightly modified (6). Overnight cultures of NR2583, NR1872, NR2589, NR2576, NR2578, and NR2670 were diluted 100-fold into fresh LB broth supplemented with 50 μg/mL carbenicillin. Cultures were grown at 37 °C to midlogarithmic phase. Cells were harvested by centrifugation at 5,000 × *g* for 10 min, as described. At this point, cells were frozen at −80 °C. Thawed cells were resuspended in 20 mM Tris·HCl (pH 7.4) supplemented with 1 mM PMSF, 100 μg/mL lysozyme, and 50 μg/mL DNase I. Cells were lysed by three passages through an EmulsiFlex-C3 high-pressure cell disruptor (Avestin, Inc.), and the lysate was centrifuged at 5,000 × *g* for 10 min to remove unbroken cells. The supernatant was centrifuged at 100,000 × *g* for 1 h to pellet membranes. Resuspended membranes were solubilized in 50 mM Tris·HCl (pH 7.4), 300 mM NaCl, 10% (vol/vol) glycerol, 5 mM $MgCl_2$, and 1% *n*-dodecyl-β-D-maltopyranoside (DDM; Anatrace) at 4 °C for 1 h. Solubilized membranes were centrifuged again at 100,000 × *g* for 1 h, and the supernatant, supplemented with 10 mM imidazole, was passed twice over TALON metal affinity resin (Clontech) preequilibrated with 50 mM Tris·HCl (pH 7.4), 300 mM NaCl, 10% (vol/vol) glycerol, 0.05% DDM, and 10 mM imidazole. After washing with 40 column volumes of 50 mM Tris·HCl (pH 7.4), 300 mM NaCl, 10% (vol/vol) glycerol, 0.05% DDM, and 20 mM imidazole, protein was eluted with 50 mM Tris·HCl (pH 7.4), 300 mM NaCl, 10% (vol/vol) glycerol, 0.05% DDM, and 200 mM imidazole. Eluates were precipitated with 10% (wt/vol) trichloroacetic acid, followed by a cold acetone wash. Precipitates were resuspended in 2× SDS-PAGE sample buffer supplemented with 5% (vol/vol) β-mercaptoethanol. Samples were boiled for 10 min and loaded onto 4–20% SDS polyacrylamide gels, and the proteins were transferred onto Immun-Blot PVDF membranes (Bio-Rad) and subjected to immunoblotting using BamA (12), LptC (13), LptF (14), and LptB polyclonal antisera, followed by immunoblotting with an anti–rabbit-HRP antibody. Bands were visualized using ECL Prime Western Blotting Detection Reagent (GE Amersham) and Biomax Light Film (Kodak).

Protein Overexpression and Purification for ATPase Assay. The pET22/42LptB-His_8, pET22/42LptB-E163Q-His_8, pET22/42LptB-H195A-His_8, pET23/42LptB-F90A-His_8, and pET23/42LptB-F90Y-His_8 plasmids were each transformed into KRX cells. Cultures were grown at 37 °C after diluting overnight cultures 100-fold into fresh LB broth supplemented with 50 μg/mL carbenicillin. LptB-His variant expression was induced with 0.2% (wt/vol) L-rhamnose at an OD_{600} of ∼1, and cultures were grown for 16 h at 16 °C. Proteins were purified as described below in the section on LptB overexpression and purification for crystallography.

To overexpress and purify the inner membrane complex, KRX cells were transformed with pCDFDuet-His_6LptB-LptFG and pET22/42LptC. Cultures were grown at 37 °C after diluting overnight cultures 100-fold into fresh LB broth supplemented with 50 μg/mL spectinomycin and 50 μg/mL carbenicillin. Complex expression was induced with 0.02% (wt/vol) L-rhamnose at an OD_{600} of ∼1, and cultures were grown for 3 h at 37 °C. Cells were harvested by centrifugation at 5,200 × *g* for 15 min and resuspended in 50 mM Tris·HCl (pH 7.4), supplemented with 1 mM PMSF, 100 μg/mL lysozyme, and 50 μg/mL DNase I. Harvested cells were lysed by three passages through an EmulsiFlex-C3 high-pressure cell disruptor. After removal of unbroken cells, membranes were recovered by centrifugation at 100,000 × *g* for 1 h. Membranes were resuspended and subsequently solubilized in 20 mM Tris·HCl (pH 7.4), 5 mM $MgCl_2$, 300 mM NaCl, 1% DDM, 10% (vol/vol) glycerol, and 2 mM ATP at 4 °C for 1 h, followed by centrifugation at 100,000 × *g* for 30 min. The supernatant was applied to TALON metal affinity resin, followed by elution with 20 mM Tris·HCl (pH 7.4), 300 mM NaCl, 0.05% DDM, 10% (vol/vol) glycerol, and 25 mM imidazole. The eluate was concentrated with an Amicon centrifugation filter, 50-kDa molecular weight cutoff (MWCO, Amicon Ultra; Millipore), and then subjected to size exclusion chromatography on a Superdex 200 10/300 GL column (GE Healthcare) in 20 mM Tris·HCl (pH 7.4), 300 mM NaCl, 0.05% DDM, and 10% (vol/vol) glycerol. Fractions were pooled and concentrated to ∼2.5 mg/mL.

LptB Overexpression and Purification for Crystallography. Full-length LptB with a C-terminal His_8 tag (henceforth referred to as LptB-His) was overexpressed as previously described (15), with a few notable changes. Cultures of BL21(λDE3) cells containing the plasmid with LptB-His were grown at 37 °C after diluting an overnight culture 100-fold into fresh LB broth supplemented with 50 μg/mL carbenicillin. Cells were grown to an OD_{600} of ∼1, and the temperature was reduced to 16 °C. Overexpression was induced by addition of 100 μM IPTG, and the cells were grown for 16 h at 16 °C. Cells were harvested by centrifugation at 5,000 × *g* for 20 min. Cells were resuspended in Tris-buffered saline [TBS; 20 mM Tris (pH 8.0), 150 mM NaCl], 20% (vol/vol) glycerol, and 0.5 mM Tris(hydroxypropyl)phosphine (THP; EMD Millipore) supplemented with 0.5 mM PMSF, 50 μg/mL lysozyme, and 50 μg/mL DNase I. Cells were lysed by three passages through a French pressure cell (Thermo Electron) at 16,000 psi and centrifuged at 6,000 × *g* for 10 min to remove unbroken cells. The supernatant was centrifuged at 100,000 × *g* for 30 min to remove membranes. Imidazole was then added to the supernatant to a final concentration of 10 mM. Ni-NTA Superflow resin (Qiagen) was prewashed with TBS supplemented with 20% (vol/vol) glycerol and 10 mM imidazole in preparation for batch nickel affinity chromatography. The supernatant was then incubated with the prewashed Ni-NTA Superflow resin at 4 °C for 1 h. Following removal of the flow-through, the resin was washed with 20 column volumes of TBS with 20% (vol/vol) glycerol and 20 mM imidazole. The protein was then eluted in one batch with two column volumes of TBS with 20% (vol/vol) glycerol, 0.5 mM THP, and 200 mM imidazole. The eluate was concentrated with an Amicon centrifugation filter at 10-kDa MWCO to ∼20 mg/mL. The concentrated

protein was further purified by size exclusion chromatography on a Superdex 200 10/300 GL column in TBS, 20% (vol/vol) glycerol, and 0.5 mM THP. The fractions with pure LptB-His were collected, pooled, and concentrated to 15–20 mg/mL using a centrifugal filter.

LptB-E163Q-His was overexpressed in KRX cells in LB supplemented with 50 μg/mL carbenicillin. Cells were induced with 0.2% L-rhamnose. Cells were harvested, and the protein was purified as described above for the wild-type protein with one notable difference. Following elution from the Ni-NTA Superflow resin and before concentration, EDTA was added to the eluate to a final concentration of 1 mM.

Native Crystals. Before crystallization, LptB-His or LptB-E163Q-His was diluted to 7–10 mg/mL with TBS to yield a final glycerol content of 10% (vol/vol). Crystals were grown with the hanging drop method at room temperature. Before setting up hanging drops, LptB-His was incubated with 2.5 mM ATP and 2.5 mM $MgCl_2$, and LptB-E163Q-His was incubated with 2.5 mM ATP at 4 °C for 1 h. After screening many conditions, the optimal condition for obtaining Mg^{2+}/ADP co-complex crystals was mixing 1 μL of protein with 1 μL of reservoir solution containing 0.1 M MES (pH 6.5) and 30% (wt/vol) PEG 4000. After several days, triangular plate-like crystals appeared. Crystals were flash-frozen with liquid nitrogen after cryoprotection with a solution containing 0.1 M MES (pH 6.5), 33% (wt/vol) PEG 4000, and 24% (vol/vol) glycerol. After screening conditions to crystallize LptB-E163Q-His in complex with ATP, the best condition was found to be mixing 1 μL of protein with 1 μL of reservoir solution containing 0.6 M NaCl, 0.1 M MES (pH 7.0), and 26.5% (wt/vol) PEG 4000. After several days, large crystals were obtained. Crystals were flash-frozen in a cryoprotectant containing 0.6 M NaCl, 0.09 M MES (pH 7.0), 28% (wt/vol) PEG 4000, 23% (vol/vol) glycerol, and 2.5 mM ATP.

Selenomethionine Derivative Purification and Crystallization. A selenomethionine (SeMet) derivative of LptB-His (henceforth called SeMet-LptB-His) was overexpressed in BL21(λDE3) from the same pET22/42 vector as the wild-type protein but was overexpressed in SeMet minimal medium, using a previously reported method (16). The protein was purified in the same buffer as described above, and the final protein solution was diluted to 7–10 mg/mL with a final glycerol content of 10% (vol/vol). Optimal crystals were obtained with 2 μL of protein mixed with 1 μL of reservoir solution composed of 0.1 M MES (pH 6.5) and 31% (wt/vol) PEG 4000. These flat, plate-like crystals were flash-frozen in a cryoprotectant containing 0.1 M MES (pH 6.5), 35% (wt/vol) PEG 4000, and 20% (vol/vol) glycerol.

Heavy Metal Soak. A tantalum derivative of the native LptB-His crystals was prepared to obtain additional phasing information. Crystals were soaked overnight with tantalum clusters (Jena) and then frozen in tantalum-free cryoprotectant, as described above.

Data Collection. SeMet-LptB-His crystals were collected at 0.97917 Å, and the crystals soaked with tantalum clusters were collected at 1.2548 Å. All other crystals were collected at 1.075 Å. LptB-His and all of its derivatives belong to the space group $C121$. LptB-E163Q-His belongs to the space group $C222_1$.

Data Processing and Structure Determination of the LptB Structure. All datasets were indexed and integrated using iMosflm (17) and scaled using Scala (18). Heavy atom sites in the SeMet and tantalum structures were determined using HKL2MAP (19). The top occupancy sites for each of the two derivatives were then input into the CCP4 (20) program Phaser (21) to refine and find additional sites using single-wavelength anomalous diffraction. Initially, only low-resolution (3.25 Å) native data were obtained, and this dataset was merged with the 2.05-Å SeMet dataset truncated to 2.5 Å and the tantalum dataset. Phases going out to 2.5 Å were obtained by multiple isomorphous replacement with anomalous scattering using SHARP (22) with the merged dataset and the Phaser-refined heavy atom sites for the two derivatives. After obtaining the phases from SHARP and performing density modification using Density Modification (DM) (23), a map that looked protein-like was obtained, but it was not sufficiently clear to facilitate model building. Therefore, Phenix Autobuild (24) was used to build a model using the experimental phases, the 2.05-Å SeMet structure factors, and the amino acid sequence of the construct. After this initial Autobuild run, a model with an R_{work} of 36.3% and an R_{free} of 40.0% was obtained. The density was much improved, but there were still several gaps in the backbone of the model. At this point, we used a homology model to fill in the gaps. Using the Wide Search Molecular Replacement server (25), we determined the optimal homology model to be Protein Data Bank ID code 1gaj. After superposition in Coot (26, 27), the missing parts of our model were manually added from the homology structure. Then, a second round of Autobuild was performed using the latest SeMet-LptB-His model to generate the map, along with the Hendrickson–Lattman coefficients from SHARP to guide the building and refinement. At this stage, a model with an R_{work} of 25.2% and an R_{free} of 30.3% was obtained. Next, the model was refined with the Crystallography and NMR System (28, 29) by doing rounds of *B*-factor refinement and simulated annealing. The refinement was then completed with Phenix by doing cycles of minimization, ADP (atomic displacement parameter or *B*-factor) refinement, and translation/libration/screw (TLS) refinement using TLS parameters determined by the TLS Motion Determination server (30), interspersed with manual adjustments using Coot. The final R_{work} and R_{free} were 21.3% and 25.2%, respectively, for the SeMet structure.

Structure Determination and Refinement of the High-Resolution Native LptB-ADP Complex. After determining the structure of the SeMet-LptB-Mg^{2+}-ADP complex, we were able to obtain a high-resolution dataset of native LptB-Mg^{2+}-ADP. We determined the structure of the native Mg^{2+}-ADP co-complex by molecular replacement using the SeMet structure as the search model and doing rigid body refinement in Phenix (31), after copying and extending the free-*R* column from the SeMet dataset. The structure was then refined in Phenix as described above. The final R_{work} and R_{free} values were 19.8% and 21.8%, respectively.

Structure Determination and Refinement of the LptB-E163Q-ATP Structure. The LptB-E163Q-ATP structure was solved by molecular replacement using Phaser with the native LptB-Mg^{2+}-ADP structure as the search model. The search model had to be broken down into the RecA-like ATPase domain and the α-helical domain to obtain a solution. Each domain was searched for twice, leading to an initial dimer model of the full protein. The model was then refined using Phenix as described above. Final R_{work} and R_{free} values of 18.8% and 21.0%, respectively, were obtained.

1. Silhavy TJ, Berman ML, Enquist LW (1984) *Experiments with Gene Fusions* (Cold Spring Harbor Laboratory Press, Cold Spring Harbor, NY).
2. Yu D, et al. (2000) An efficient recombination system for chromosome engineering in Escherichia coli. *Proc Natl Acad Sci USA* 97(11):5978–5983.
3. Reynolds CM, Raetz CR (2009) Replacement of lipopolysaccharide with free lipid A molecules in Escherichia coli mutants lacking all core sugars. *Biochemistry* 48(40):9627–9640.
4. Datsenko KA, Wanner BL (2000) One-step inactivation of chromosomal genes in Escherichia coli K-12 using PCR products. *Proc Natl Acad Sci USA* 97(12):6640–6645.

5. Cherepanov PP, Wackernagel W (1995) Gene disruption in Escherichia coli: TcR and KmR cassettes with the option of Flp-catalyzed excision of the antibiotic-resistance determinant. *Gene* 158(1):9–14.
6. Chng SS, Gronenberg LS, Kahne D (2010) Proteins required for lipopolysaccharide assembly in Escherichia coli form a transenvelope complex. *Biochemistry* 49(22):4565–4567.
7. Chung CT, Miller RH (1993) Preparation and storage of competent Escherichia coli cells. *Methods Enzymol* 218:621–627.
8. de Boer PA, Crossley RE, Rothfield LI (1989) A division inhibitor and a topological specificity factor coded for by the minicell locus determine proper placement of the division septum in E. coli. *Cell* 56(4):641–649.
9. Sherman DJ, Okuda S, Denny WA, Kahne D (2013) Validation of inhibitors of an ABC transporter required to transport lipopolysaccharide to the cell surface in Escherichia coli. *Bioorg Med Chem* 21(16):4846–4851.
10. Sklar JG, et al. (2007) Lipoprotein SmpA is a component of the YaeT complex that assembles outer membrane proteins in Escherichia coli. *Proc Natl Acad Sci USA* 104(15):6400–6405.
11. Ruiz N, Falcone B, Kahne D, Silhavy TJ (2005) Chemical conditionality: A genetic strategy to probe organelle assembly. *Cell* 121(2):307–317.
12. Kim S, et al. (2007) Structure and function of an essential component of the outer membrane protein assembly machine. *Science* 317(5840):961–964.
13. Freinkman E, Okuda S, Ruiz N, Kahne D (2012) Regulated assembly of the transenvelope protein complex required for lipopolysaccharide export. *Biochemistry* 51(24):4800–4806.
14. Villa R, et al. (2013) The Escherichia coli Lpt transenvelope protein complex for lipopolysaccharide export is assembled via conserved structurally homologous domains. *J Bacteriol* 195(5):1100–1108.
15. Gronenberg LS, Kahne D (2010) Development of an activity assay for discovery of inhibitors of lipopolysaccharide transport. *J Am Chem Soc* 132(8):2518–2519.
16. Van Duyne GD, Standaert RF, Karplus PA, Schreiber SL, Clardy J (1993) Atomic structures of the human immunophilin FKBP-12 complexes with FK506 and rapamycin. *J Mol Biol* 229(1):105–124.
17. Leslie AGW, Powell HR (2007) Processing diffraction data with Mosflm. *Evolving Methods for Macromolecular Crystallography* 235:41–51.
18. Evans P (2006) Scaling and assessment of data quality. *Acta Crystallogr D Biol Crystallogr* 62(Pt 1):72–82.
19. Pape T, Schneider TR (2004) HKL2MAP: a graphical user interface for macromolecular phasing with SHELX programs. *Journal of Applied Crystallography* 37:843–844.
20. Bailey S; Collaborative Computational Project, Number 4 (1994) The CCP4 suite: Programs for protein crystallography. *Acta Crystallogr D Biol Crystallogr* 50(Pt 5):760–763.
21. McCoy AJ, et al. (2007) Phaser crystallographic software. *J Appl Cryst* 40(Pt 4):658–674.
22. Bricogne G, Vonrhein C, Flensburg C, Schiltz M, Paciorek W (2003) Generation, representation and flow of phase information in structure determination: Recent developments in and around SHARP 2.0. *Acta Crystallogr D Biol Crystallogr* 59(Pt 11): 2023–2030.
23. Cowtan K (1994) *Joint CCP4 and ESF-EACBM Newsletter on Protein Crystallography*, pp 34–38.
24. Terwilliger TC, et al. (2008) Iterative model building, structure refinement and density modification with the PHENIX AutoBuild wizard. *Acta Crystallogr D Biol Crystallogr* 64(Pt 1):61–69.
25. Stokes-Rees I, Sliz P (2010) Protein structure determination by exhaustive search of Protein Data Bank derived databases. *Proc Natl Acad Sci USA* 107(50):21476–21481.
26. Emsley P, Cowtan K (2004) Coot: Model-building tools for molecular graphics. *Acta Crystallogr D Biol Crystallogr* 60(Pt 12 Pt 1):2126–2132.
27. Emsley P, Lohkamp B, Scott WG, Cowtan K (2010) Features and development of Coot. *Acta Crystallogr D Biol Crystallogr* 66(Pt 4):486–501.
28. Brünger AT, et al. (1998) Crystallography & NMR system: A new software suite for macromolecular structure determination. *Acta Crystallogr D Biol Crystallogr* 54(Pt 5): 905–921.
29. Brunger AT (2007) Version 1.2 of the Crystallography and NMR system. *Nat Protoc* 2(11):2728–2733.
30. Painter J, Merritt EA (2006) Optimal description of a protein structure in terms of multiple groups undergoing TLS motion. *Acta Crystallogr D Biol Crystallogr* 62(Pt 4): 439–450.
31. Adams PD, et al. (2010) PHENIX: A comprehensive Python-based system for macromolecular structure solution. *Acta Crystallogr D Biol Crystallogr* 66(Pt 2):213–221.

A

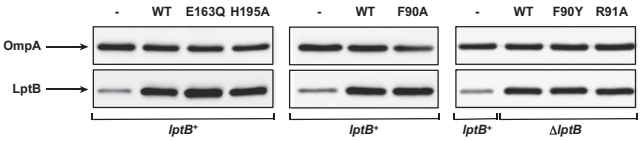

B

Dominant effect of LptB-His$_8$ variants in merodiploid strains

Plasmid	Zone of inhibition (in mm)			
	Bacitracin	Novobiocin	Erythromycin	Rifampin
pET23/42LptB-His$_8$	<6	[8]	[9]	9
pET23/42LptB-E163Q-His$_8$	<6	**10**	**11**	**12**
pET23/42LptB-H195A-His$_8$	**9**	**12**	**10 [12]**	**12**
pET23/42LptB-F90A-His$_8$	<6	[8]	[8]	8

C

OM permeability of haploid strains producing LptB-His$_8$ variants

AA change	Zone of inhibition (in mm)			
	Bacitracin	Novobiocin	Erythromycin	Rifampin
None (WT)	11	15[24]	10[19]	12
F90Y	**14**	**18[23]**	**14[18]**	**14**
R91A	11	15[23]	10[17]	12

Fig. S1. Genetic analysis of LptB variants. (*A*) Western blots of LptB derivatives reveal that the specific changes do not alter cellular levels of LptB. OmpA is shown as a loading control. Nonfunctional variants are expressed in merodiploid strains harboring pET23/42LptB derivatives and the wild-type *lptB* chromosomal allele. The samples for the functional LptB variants (F90Y and R91A) are from haploid strains harboring pET23/42LptB-F90Y and pET23/42LptB-R91A. Wild-type haploid strain (NR754), which carries the *lptB*$^+$ allele at the native chromosomal locus, is marked with "-"; amino acid changes encoded in plasmids are labeled above the lanes; and parent plasmids are labeled "WT." Chromosomal *lptB* alleles of strains are indicated below the lanes. (*B*) Table shows zones of inhibition, as measured by disk diffusion assays, of merodiploid strains carrying the *lptB*$^+$ allele at the native chromosomal locus and the indicated plasmids encoding LptB variants. Diffusion assays were performed with 6-mm disks. Numbers outside brackets represent the diameter (in millimeters) of the zone of total growth inhibition. Numbers inside brackets represent the diameter (in millimeters) of the zone of partial growth inhibition. Increased sensitivity with respect to the parent strain is shown in bold. (*C*) OM permeability of haploid strains producing LptB-His$_8$ variants and carrying the Δ*lptB* allele at the native chromosomal locus. Diffusion assays were performed as described in *B*. The increased sensitivity to antibiotics reported here is recessive to the wild-type *lptB* allele. AA, amino acid.

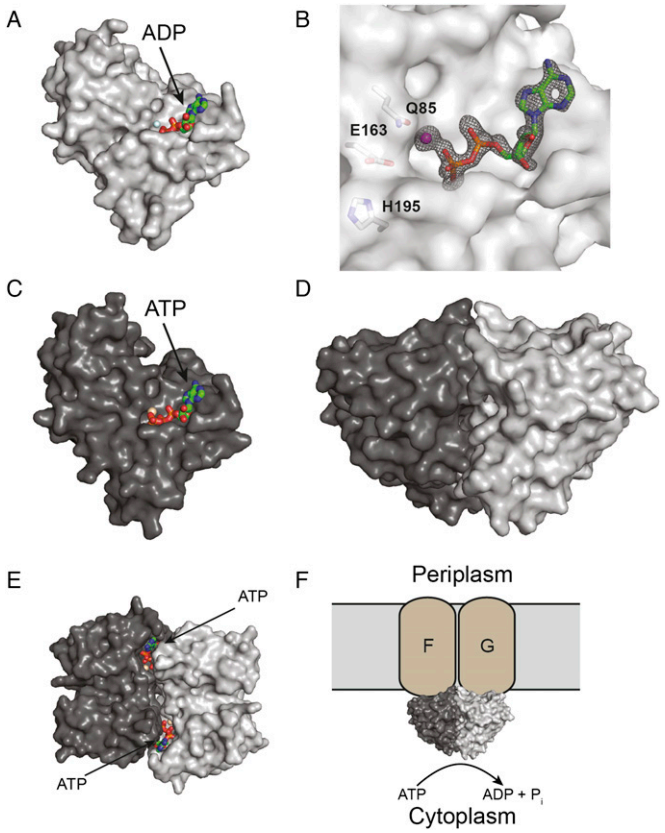

Fig. S2. Crystallographic analysis of LptB-ADP and LptB-ATP. (*A*) Native LptB with a C-terminal His_8 tag crystallized with ADP-Mg^{2+} bound in the active site. (*B*) F_o-F_c omit map of ADP-Mg^{2+} from the LptB-ADP structure is contoured at 3σ and shows clear electron density for two phosphate groups. The side chains of Q85, E163, and H195 are illustrated as sticks. (*C*) Catalytically inactive variant of LptB bound to ATP crystallized in a different crystal form. (*D*) LptB-ATP crystallized as a canonical nucleotide-sandwich dimer after taking into account symmetry mates. (*E*) Top view of the nucleotide-sandwich dimer shows ATP molecules sandwiched between each protomer. (*F*) Based on comparisons with other nucleotide-binding domain structures, we can predict where transmembrane domains LptF (F) and LptG (G) might reside relative to the active LptB dimer.

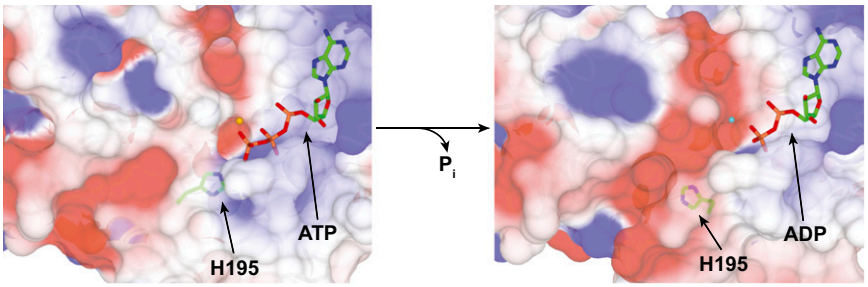

Fig. S3. Electrostatic potential surface of LptB-ATP. Nucleotides and the side chain of H195 are shown as sticks to indicate structural changes between ATP-bound and ADP-bound structures. Sodium and magnesium ions are depicted as light orange and light cyan spheres, respectively. The electrostatic potential surface generated in CCP4mg (1) is shown. Blue represents areas of positive charge, and red represents areas of negative charge. P_i, inorganic phosphate.

1. McNicholas S, Potterton E, Wilson KS, Noble ME (2011) Presenting your structures: The CCP4mg molecular-graphics software. *Acta Crystallogr D Biol Crystallogr* 67(Pt 4):386–394.

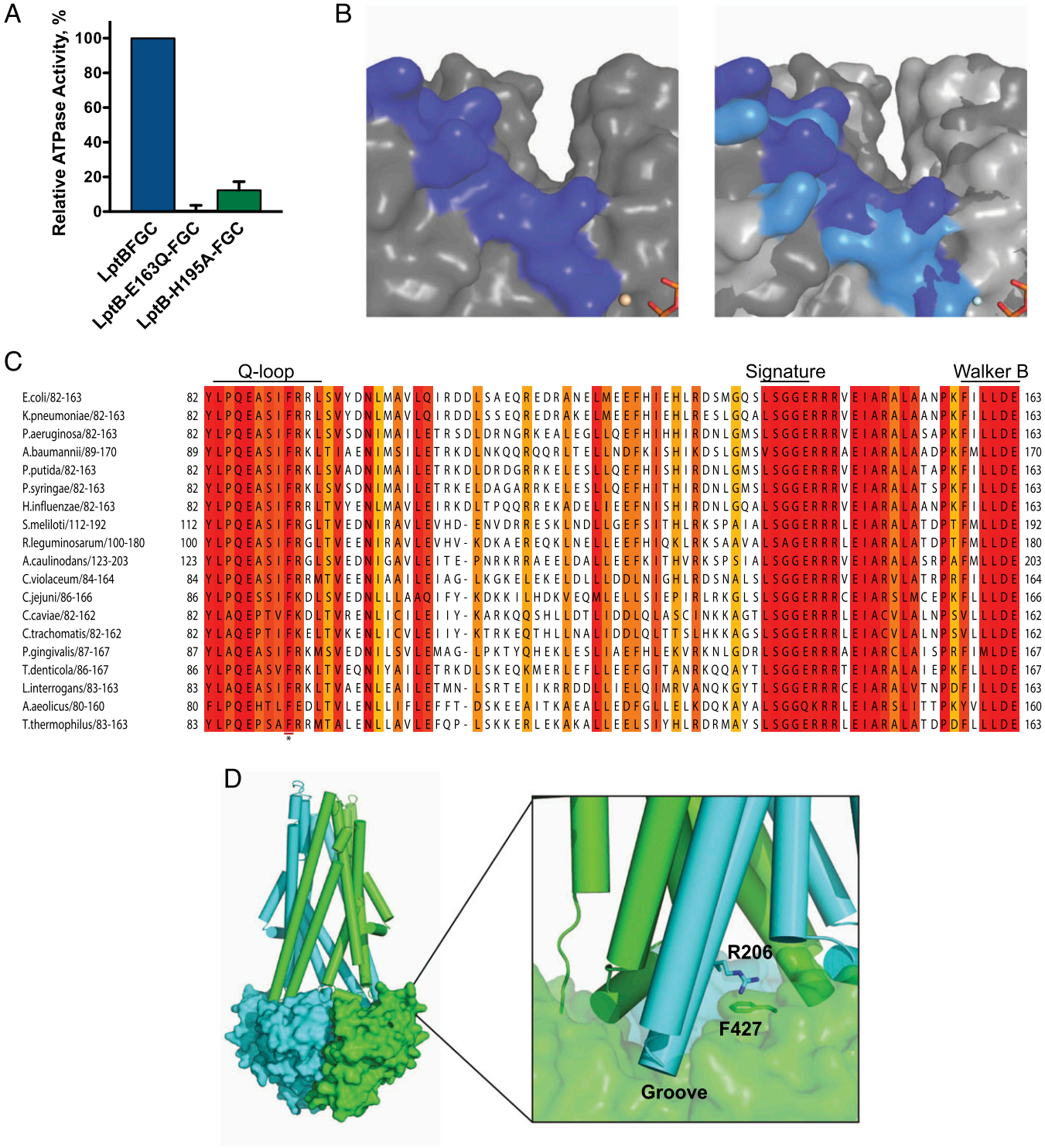

Fig. S4. Analysis of full inner membrane (IM) complex and groove analysis of LptB. (*A*) $LptB_2FGC$ variants were overexpressed and purified, and their ATPase activity was measured with 5 mM ATP/$MgCl_2$. Bars represent the average of three experiments, with error bars indicating SDs. (*B*) Surface representations of LptB-ATP, depicted in dark gray (*Left*), and LptB-ADP, depicted in light gray and overlaid on the LptB-ATP structure (*Right*), highlight the groove region. The Q-loop region is depicted in shades of blue (dark blue in LptB-ATP, light blue in the LptB-ADP) in both structures to demonstrate conformational changes resulting from ATP hydrolysis. (*C*) Sequence alignment of the structurally diverse region of LptB orthologs. Alignment shows conservation as determined by ClustalW (1, 2). Conserved residues are highlighted using JalView (3) by conservation scores (range of 1–10, with 10 being the highest conservation; 7 = yellow, 7 > orange > 10, 10 = red). Accession numbers of sequences used in the alignment are as follows: NP_417668 (*Escherichia coli*), WP_017899918 (*Klebsiella pneumoniae*), NP_253151 (*Pseudomonas aeruginosa*), YP_001714311 (*Acinetobacter baumannii*), NP_743114 (*Pseudomonas putida*), NP_794206 (*Pseudomonas syringae*), P45073 (*Haemophilus influenzae*), P25885 (*Sinorhizobium meliloti*), AAA80299 (*Rhizobium leguminosarum*), P33982 (*Azorhizobium caulinodans*), AAQ60995 (*Chromobacterium violaceum*), CAC19930 (*Campylobacter jejuni*), NP_828894 (*Chlamydophila caviae*), NP_220172 (*Chlamydia trachomatis*), AAQ65812 (*Porphyromonas gingivalis*), NP_971258 (*Treponema denticola*), YP_001503 (*Leptospira interrogans*), NP_213289 (*Aquifex aeolicus*), and YP_004046

Legend continued on following page

(*Thermus thermophilus*). Residue F90 in *E. coli* LptB is indicated with a line and asterisk below the column with its position. (*D*) Crystal structure of Sav1866 bound to a nonhydrolyzable ATP analogue (Protein Data Bank ID code 2onj). (*Left*) Overall structure of the homodimeric multidrug exporter, with one chain shown in green and the other shown in cyan. Nucleotide-binding domains are depicted as surfaces, and transmembrane domains are depicted as cylinders. (*Right*, *Inset*) Close-up view of the side of the transporter, highlighting a π-cation interaction between R206 in one transmembrane domain and F427 in one nucleotide-binding domain. F427 structurally aligns with F90 in LptB.

1. Goujon M, et al. (2010) A new bioinformatics analysis tools framework at EMBL-EBI. *Nucleic Acids Res* 38(Web Server issue):W695-9.
2. Larkin MA, et al. (2007) Clustal W and Clustal X version 2.0. *Bioinformatics* 23(21):2947–2948.
3. Waterhouse AM, Procter JB, Martin DM, Clamp M, Barton GJ (2009) Jalview Version 2—A multiple sequence alignment editor and analysis workbench. *Bioinformatics* 25(9):1189–1191.

Table S1. Strains used in this study

Strain	Genotype	Source
BL21(λDE3)	F$^-$ *omp*T *gal dcm lon hsd*S$_B$(r$_B^-$, m$_B^-$) λ(DE3)	Novagen
KRX	[F′, *tra*D36, Δ*omp*P, *pro*A$^+$B$^+$, *lac*I^q, Δ(*lac*Z)M15] Δ*omp*T, *end*A1, *rec*A1, *gyr*A96, *thi*-1, *hsd*R17 (r$_K^-$, m$_K^+$), e14$^-$ (McrA$^-$), *rel*A1, *sup*E44, Δ(*lac-pro*AB), Δ(*rha*BAD)::T7 gene 1	Promega
NovaBlue	*endA1 hsd*R17 (r$_K^-$, m$_K^+$) *sup*E44 *thi*-1 *rec*A1 *gyr*A96 *rel*A1 *lac* F′[*pro*A$^+$B$^+$ *lac*I^{q}ZΔM15::Tn*10*]	Novagen
DH5α	F$^-$ Φ80*lac*ZΔM15 Δ(*lac*ZYA-*arg*F) U169 *rec*A1 *end*A1 *hsd*R17 (r$_K^-$, m$_K^+$) *pho*A *sup*E44 λ$^-$ *thi*-1 *gyr*A96 *rel*A1	Life Technologies
DY378	W3110 λcI857 Δ(*cro-bioA*)	Yu et al. (1)
MC4100	F$^-$ *araD139* Δ(*arg*F-*lac*)U169 *rpsL150 relA1 flbB5301 deoC1 ptsF25 rbsR*	Casadaban (2)
NR754	MC4100 *ara*$^+$	Ruiz et al. (3)
NR1414	NR754 (pET23/42)	This study
NR1818	DY378 (pWSK29LptCAB)	This study
NR1846	DY378 Δ*lptB*::*kan* (pWSK29LptCAB)	This study
NR1872	NR754 (pET23/42LptB-His8)	This study
NR1890	NR1872 Δ*lptB*::*kan*	This study
NR1926	DY378 (pRC7LptB)	This study
NR1931	DY378 (pRC7KanLptB)	This study
NR2050	NR754 Δ*lptB tet2* (pRC7KanLptB)	This study
NR2093	NR754 Δ*lptB tet2* (pET23/42LptB-His$_8$)	This study
NR2101	NR754 Δ*lptB tet2* (pET23/42LptB)	This study
NR2583	NR754 (pET23/42LptB)	This study
NR2571	NR2050 (pET23/42LptB-F90A)	This study
NR2575	NR754 (pET23/42LptB-F90A)	This study
NR2572	NR2050 (pET23/42LptB-F90A-His$_8$)	This study
NR2576	NR754 (pET23/42LptB-F90A-His$_8$)	This study
NR2573	NR754 Δ*lptB tet2* (pET23/42LptB-F90Y)	This study
NR2577	NR754 (pET23/42LptB-F90Y)	This study
NR2574	NR754 Δ*lptB tet2* (pET23/42LptB-F90Y-His$_8$)	This study
NR2578	NR754 (pET23/42LptB-F90Y-His$_8$)	This study
NR2605	NR754 Δ*lptB tet2* (pET23/42LptB-R91A)	This study
NR2634	NR754 (pET23/42LptB-R91A)	This study
NR2674	NR754 Δ*lptB tet2* (pET23/42LptB-R91A-His$_8$)	This study
NR2675	NR754 (pET23/42LptB-R91A-His$_8$)	This study
NR2722	NR2050 (pET23/42LptB-E163Q)	This study
NR2723	NR754 (pET23/42LptB-E163Q)	This study
NR2586	NR2050 (pET23/42LptB-E163Q-His$_8$)	This study
NR2589	NR754 (pET23/42LptB-E163Q-His$_8$)	This study
NR2718	NR2050 (pET23/42LptB-H195A)	This study
NR2719	NR754 (pET23/42LptB-H195A)	This study
NR2669	NR2050 (pET23/42LptB-H195A-His$_8$)	This study
NR2670	NR754 (pET23/42LptB-H195A-His$_8$)	This study

1. Yu D, et al. (2000) An efficient recombination system for chromosome engineering in Escherichia coli. *Proc Natl Acad Sci USA* 97(11):5978–5983.
2. Casadaban MJ (1976) Transposition and fusion of the *lac* genes to selected promoters in *Escherichia coli* using bacteriophage *lambda* and *Mu*. *J Mol Biol* 104(3):541–555.
3. Ruiz N, Gronenberg LS, Kahne D, Silhavy TJ (2008) Identification of two inner-membrane proteins required for the transport of lipopolysaccharide to the outer membrane of Escherichia coli. *Proc Natl Acad Sci USA* 105(14):5537–5542.

Table S2. SDM primers

Amino acid change	Primer name	Primer sequence (5′ to 3′)
Stop codon insertion	LptB-MinusCHis-f	GAAGACTTCAGACTCTGAGAGCACCACCACCACCACCAC
	LptB-MinusCHis-r	GTGGTGGTGGTGGTGGTGCTCTCAGAGTCTGAAGTCTTC
F90A	5LptBF90A	GCCACAGGAAGCCTCCATTGCCCGTCGCCTC
	3LptBF90A	GAGGCGACGGGCAATGGAGGCTTCCTGTGGC
F90Y	5LptBF90Y	CCACAGGAAGCCTCCATTTACCGTCGCCTC
	3LptBF90Y	GAGGCGACGGTAAATGGAGGCTTCCTGTGG
R91A	5LptBR91A	ACAGGAAGCCTCCATTTTCGCTCGCCTCAGCGTT
	3LptBR91A	AACGCTGAGGCGAGCGAAAATGGAGGCTTCCTGT
E163Q	LptB-E163Q-f	TATTCTGCTCGACCAACCGTTTGCCGGGGTTGACCCG
	LptB-E163Q-r	CGGGTCAACCCCGGCAAACGGTTGGTCGAGCAGAATA
H195A	LptB-H195A-f	CAGTGTTTCACGCACGTTGGCGTCAGTGATCAGCACGCC
	LptB-H195A-r	GGCGTGCTGATCACTGACGCCAACGTGCGTGAAACACTG

Table S3. Other primers

Primer name	Primer Sequence (5′ to 3′)
5LptBP1	GTCGCAGCTGCAGGACAAAAACAACAAAGGCCAGACCCCGGCACAGAA GAAGGGTAATTAATTCGTTATGGTGTAGGCTGGAGCTGCTTC
3LptBP2	CTGAGTTGCAAACCTTGCTTCATGTTCAGAATCGTACTCTCCTGCTAAAACGTC GCAAACTTCTACCCTACATATGAATATCCTCCTTA
5LptBEcoRI	ACCGGAATTCAGGAGGTTCGTTATGGCAACATTAACTGC
3LptBHindIII	AGCAAGCTTCAGAGTCTGAAGTCTTC
blaP1	ATGAGTATTCAACATTTCCGTGTCGCCCTTATTCCCTTTTTTGCGGCATTTTGC CTTCCTGTTTTTGCTCGTGTAGGCTGGAGCTGCTTC
blaP2	TTACCAATGCTTAATCAGTGAGGCACCTATCTCAGCGATCTGTCTATTTCGTTCAT CCATAGTTGCCTGACATATGAATATCCTCCTTA
N-NcoI-His_6LptB	TATACCATGGGCCATCATCATCATCATCACGGAATGGCAACATTAACTGCAAAGAACC
C-LptB-EcoRI	TATAGAATTCTCAGAGTCTGAAGTCTTCCCCAAGGTATACACG
N-NdeI-LptC	TATACATATGAGTAAAGCCAGACGTTGGG
C-LptC-HindIII	TATAAAGCTTTTAAGGCTGAGTTTGTTTGTTTTGAATTTC

Table S4. Data collection and refinement statistics

Dataset	LptB-ADP	LptB-ATP
Space group	C121	$C222_1$
Unit cell		
Dimensions (a, b, c), Å	191.90, 36.02, 64.51	66.62, 138.36, 101.28
Angles (α, β, γ), °	90.00, 96.16, 90.00	90, 90, 90
Data collection*		
Wavelength, Å	1.075	1.075
Resolution range, Å	40.41–1.55 (1.63–1.55)	40.86–1.65 (1.74–1.65)
R_{merge}	0.074 (0.570)	0.139 (0.806)
Completeness, %	98.6 (94.7)	99.2 (98.5)
Mean $I/\sigma(I)$	9.8 (2.1)	9.2 (2.8)
Unique reflections	63,317	56,004
Multiplicity	3.9 (3.4)	7.9 (8.0)
Refinement		
R_{work}, %/R_{free},%	19.76/21.76	18.81/21.00
No. of LptB molecules per asymmetrical unit	2	2
No. of modeled LptB residues per chain	234 (A)/230 (B)	235 (A)/235 (B)
No. of water molecules	168	149
No. of ions	2	2
Average *B*-factor, $Å^2$		
Nucleotide-metal	25.876	14.869
Solvent	32.795	28.792
Protein	29.666	25.95
Ramachandran plot		
Favored, %	99.8	98.3
Disallowed, %	0	0
rmsd from ideal geometry		
Bond lengths, Å	0.004	0.007
Bond angles, °	0.95	0.965

*Values in parentheses are for the shell with the highest resolution.

Table S5. Data collection and phasing statistics

Dataset	LptB-ADP (SeMet)	LptB-ADP (Tantalum)	LptB-ADP (Low-resolution native)
Space group	C121	C121	C121
Unit cell			
Dimensions (a, b, c), Å	192.60, 35.88, 64.34	192.31, 36.79, 64.43	194.55, 35.39, 65.15
Angles (α, β, γ), °	90, 95.83, 90	90, 95.08, 90	90, 95.37, 90
Data collection*			
Wavelength, Å	0.97917	1.2548	1.075
Resolution range, Å	40–2.05 (2.16–2.05)	47.89–2.80 (2.95–2.80)	48.42–3.25 (3.43–3.25)
R_{merge}	0.074 (0.498)	0.097 (0.378)	0.182 (0.380)
Completeness, %	99.2 (97.8)	99.6 (99.6)	98.8 (99.3)
Mean $I/\sigma(I)$	8.7 (2.3)	8.3 (3.0)	3.8 (2.2)
Unique reflections	27,803	11,391	7,169
Multiplicity	3.3 (3.2)	3.7 (3.7)	3.0 (3.1)
Overall isomorphous phasing power acentric	1.073	0.689	0
Overall isomorphous phasing power centric	0.906	0.673	0
Overall anomalous phasing power	0.919	0.426	0

*Values in parentheses are for the shell with the highest resolution.